PERGAMON

International Journal of Heat and Mass Transfer 45 (2002) 99–112

International Journal of HEAT and MASS TRANSFER

www.elsevier.com/locate/ijhmt

Compressible flow and heat transfer in ultracentrifuges: hybrid analysis via integral tranforms

L.M. Pereira [1], J.S. Pérez Guerrero [2], N. Brazão [3], R.M. Cotta *

Laboratory of Transmission and Technology of Heat, Mechanical Engineering Department, EE/COPPE/UFRJ, Universidade Federal do Rio de Janeiro, Cidade Universitaria C.P. 68503, Cx. Postal 68503, Rio de Janeiro, RJ 21945-970, Brazil

Received 25 May 2000; received in revised form 21 March 2001

Abstract

Compressible flow and heat transfer within gas-filled rapidly rotating cylindrical cavities is analyzed through a formal analytical solution based on the integral transform method. The axisymmetric continuity, Navier–Stokes and energy equations are handled for perturbations over the rigid body rotation solution typical of very high angular velocities, aimed at finding the secondary flow pattern induced by the end caps prescribed boundary conditions. The resulting linearized formulation in streamfunction-only form is solved through the generalized integral transform technique (GITT), and converged numerical results are obtained for streamfunction and velocity components, which are critically compared against previously reported purely discrete solutions. The physical flow behavior is also interpreted in terms of the major governing parameters. © 2001 Elsevier Science Ltd. All rights reserved.

1. Introduction

During World War II, the first experiments with gas ultracentrifuges were undertaken, aimed at the military use of enriched uranium resulting from this isotopic separation process. However, the idea of employing gravitational and/or centrifugal fields for attaining gaseous isotopic separation dates back to the end of the 19th century. After the war, and then more in connection with pacific nuclear energy applications, there was a renewed interest in this analysis, and considerable progress in the modeling and simulation of such technology was achieved [1].

By the mid 1970s and early 1980s the scientific literature was quite fertile in the analysis of gas flow behavior within rapidly rotating cylinders. By the same time, laser-induced isotopic separation appeared as an alternative for the centrifugal separation technology, slowing down somehow the scientific research on this already industrially proved mechanical approach. However, with the need of optimizing the performance of existing plants, and also in connection with the urge of developing countries in producing their own nuclear fuel, computational simulation of ultracentrifuges became a research topic of recent revival. Thus, this compressible flow and heat transfer analysis is essential in the evaluation of separation factors and separative power of the centrifuge proposed or modified configuration, to be optimized from the major operational parameters [1].

The present work is aimed at studying the countercurrent compressible gas flow within ultracentrifuges for isotopic separation. The mathematical model considers the axisymmetric continuity, Navier–Stokes and energy equations, together with the state equation for ideal gases. The linearized form of these equations is usually considered, as a result of perturbations to the rigid body rotation solution, induced by the temperature and velocity boundary conditions at the cylindrical cavity

* Corresponding author. Tel.: +55-21-562-8368; fax: +55-21-290-6626.

E-mail addresses: mariano@univap.br (L.M. Pereira), cotta@serv.com.ufrj.br (R.M. Cotta).

[1] Comissão Nacional de Energia Nuclear – CNEN, Coordenação de Rejeitos Radioativos – COREJ, Rua General Severiano, 90 Botafogo, Rio de Janeiro, RJ 22294-900, Brazil.

[2] Instituto de Pesquisa e Desenvolvimento, IP&D, Universidade do Vale do Paraíba, UNIVAP, Av. Shishima Hifumi, 2911 Urbanova, 12244-000 S.J. dos Campos, SP, Brazil.

[3] Divisão de Gasdinâmica, Centro Tecnológico da Marinha, São Paulo, SP, Brazil.

PII: S0017-9310(01)00122-3

Nomenclature

Br	Brinkman number (Eq. (6y))
c_p	specific heat at constant pressure
c_v	specific heat at constant volume
Ek	Ekman number (Eq. (6w))
G	velocity parameter (Eq. (2d))
h	aspect ratio
I_0, I_1	modified Bessel function of the first kind and zero and first order, respectively
J_0, J_1	Bessel function of the first kind and zero and first order, respectively
k	thermal conductivity
K_0, K_1	modified Bessel function of the second kind and zero and first order, respectively
M	molecular weight of the gas
P	absolute pressure of the gas
Pr	Prandtl number (Eq. (6x))
R, Z	radial and axial coordinates
r, z	dimensionless radial and axial coordinates
$\Re$	universal gas constant
T	gas absolute temperature
V_R, V_Z, V_θ	radial, axial and angular velocity components, respectively
v_r, v_z, v_θ	dimensionless radial, axial and angular velocity components, respectively

Greek symbols

$\alpha_i, \beta_m, \lambda_n$	eigenvalues
κ	radii ratio, $\kappa = R_1/R_2$
γ	ratio of specific heats, $\gamma = c_p/c_v$
μ	absolute viscosity
ν	kinematic viscosity
θ	angular coordinate
ρ	gas specific mass
ψ	dimensionless streamfunction
X_i, Γ_m, Φ_n	eigenfunctions
Θ	dimensionless temperature
Ω	angular speed of the centrifuge

end caps [1]. The generalized integral transform technique, GITT [2–5], is the solution methodology selected for this simulation task, in light of its hybrid numerical–analytical nature, which shall allow for the establishment of truly benchmark results for this challenging heat and fluid flow problem, as well as for the more computationally effective coupling with the separation calculation and with the overall optimization of this device.

A brief literature review was here undertaken to better define the scope of the present contribution. Due to its relation to a sensible technological field, the relevant literature for this problem is in general classified or at least not readily available in the archival periodicals. In light of the complex nonlinear nature of the mathematical formulation, various approximate solution paths were attempted along the years, roughly around three types of methodologies: eigenfunction expansions, boundary layers matching, and fully discrete schemes. Some of the most pertinent contributions are listed in references [6–15].

The GITT is an eigenfunction expansion approach, derived from the classical integral transformation for linear diffusion problems. Over the last two decades it has been extended to handle various classes of linear and nonlinear diffusion and convection–diffusion problems, including Navier–Stokes and boundary layer-based formulations. Some of these contributions, closely related to the scope of the present analysis, are listed in references [16–21], in particular those connected to the solution of the Navier–Stokes and energy equations in the cylindrical coordinates system [18,19]. Its hybrid nature allows for a straightforward analytical error control procedure, which facilitates the establishment of reference results in different classes of problems. Besides, the semi-analytical structure offered for the potential solutions is particularly suitable for the coupling with optimization modules in the present physical situation, when a purely discrete solution would require several re-evaluations of the whole gas dynamic flow field.

2. Problem formulation

The physical problem consists of a pure gas flow within an ultracentrifuge schematically represented in Fig. 1 below. In the specific case of uranium enrichment, this gas is UF_6, with the coexistence of the two isotopes, U-235 and U-238. Very high rotational speeds produce a separation effect in the radial direction, with the gas containing the heavier isotope being projected to the outermost boundary. The main rotational flow is perturbed by mechanical and/or thermal drives at the top and bottom caps, promoting a secondary flow which allows for the internal circulation of the radioisotope, so as to permit its mechanical separation through apertures at the centrifuge end caps.

The gas centrifuge is formed by two coaxial cylinders, with internal radius R_1 and external radius R_2, and height H, with constant angular velocity Ω, enclosing a viscous compressible gas flow. Considering the continuum hypothesis still valid for this gas flow, the modeling equations are those for conservation of mass, momentum (Navier–Stokes), and energy, together with the ideal gas equation of state, which in the cylindrical coordi-

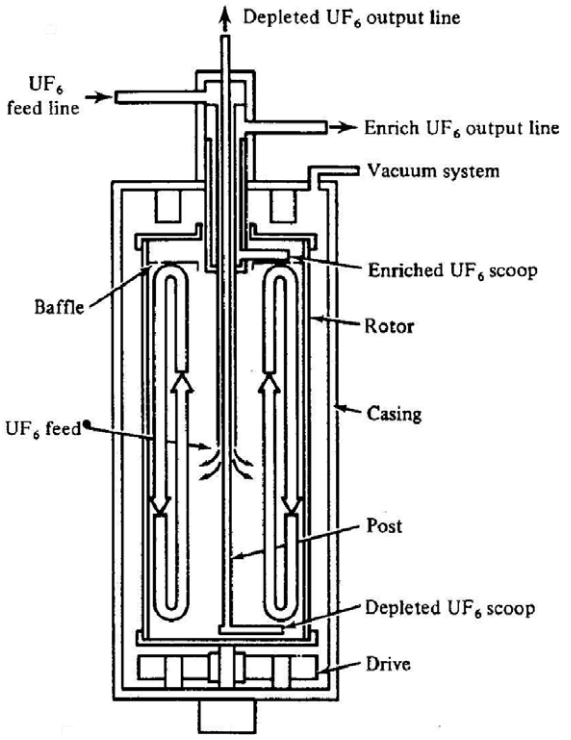

Fig. 1. Schematic representation of a gas ultracentrifuge [10].

nates system and for laminar steady regime are given by [1,11]

$$\frac{1}{R}\frac{\partial}{\partial R}(\rho R V_{\mathrm{R}}) + \frac{\partial}{\partial Z}(\rho V_Z) = 0, \tag{1a}$$

$$\rho\left(V_{\mathrm{R}}\frac{\partial V_{\mathrm{R}}}{\partial R} - \frac{V_\theta^2}{R} + V_Z\frac{\partial V_{\mathrm{R}}}{\partial Z}\right) = -\frac{\partial P}{\partial R} + \mu\left[\nabla^2 V_{\mathrm{R}} - \frac{V_{\mathrm{R}}}{R^2} + \frac{1}{3}\frac{\partial}{\partial R}(\nabla\cdot\mathbf{V})\right], \tag{1b}$$

$$\rho\left(V_{\mathrm{R}}\frac{\partial V_\theta}{\partial R} + \frac{V_{\mathrm{R}}V_\theta}{R} + V_Z\frac{\partial V_\theta}{\partial Z}\right) = \mu\left[\nabla^2 V_\theta - \frac{V_\theta}{R^2}\right], \tag{1c}$$

$$\rho\left(V_{\mathrm{R}}\frac{\partial V_Z}{\partial R} + V_Z\frac{\partial V_Z}{\partial Z}\right) = -\frac{\partial P}{\partial Z} + \mu\left[\nabla^2 V_Z + \frac{1}{3}\frac{\partial}{\partial Z}(\nabla\cdot\mathbf{V})\right], \tag{1d}$$

$$\rho c_{\mathrm{v}}\left(V_{\mathrm{R}}\frac{\partial T}{\partial R} + V_Z\frac{\partial T}{\partial Z}\right) + P(\nabla\cdot\mathbf{V}) = k\nabla^2 T + \Delta_{\mathrm{visc}}, \tag{1e}$$

$$P = \rho\frac{\Re}{M}T, \tag{1f}$$

where $\Re$ is the universal gas constant, M is the gas molecular mass, ρ is the gas specific mass, P is absolute pressure and T is the gas absolute temperature.

Eqs. (1a)–(1e) are subjected to the following boundary conditions, once the mechanical drive mode of operation is selected for analysis:

$$V_{\mathrm{R}}(R_1, Z) = 0, \tag{1g}$$
$$V_\theta(R_1, Z) = \Omega R_1, \tag{1h}$$
$$V_z(R_1, Z) = 0, \tag{1i}$$
$$T(R_1, Z) = 0, \tag{1j}$$

$$V_{\mathrm{R}}(R_2, Z) = 0, \tag{1k}$$
$$V_\theta(R_2, Z) = \Omega R_2, \tag{1l}$$
$$V_z(R_2, Z) = 0, \tag{1m}$$
$$T(R_2, Z) = 0, \tag{1n}$$

$$V_{\mathrm{R}}(R, -\tfrac{1}{2}H) = 0, \tag{1o}$$
$$V_\theta(R, -\tfrac{1}{2}H) = R(\Omega + \Delta\Omega_{\mathrm{B}}), \tag{1p}$$
$$V_z(R, -\tfrac{1}{2}H) = 0, \tag{1q}$$
$$T(R, -\tfrac{1}{2}H) = 0, \tag{1r}$$

$$V_{\mathrm{R}}(R, \tfrac{1}{2}H) = 0, \tag{1s}$$
$$V_\theta(R, \tfrac{1}{2}H) = R(\Omega + \Delta\Omega_{\mathrm{T}}), \tag{1t}$$
$$V_z(R, \tfrac{1}{2}H) = 0, \tag{1u}$$
$$T(R, \tfrac{1}{2}H) = 0, \tag{1v}$$

where $\Delta\Omega_{\mathrm{B}}$ and $\Delta\Omega_{\mathrm{T}}$ represent the differential rotations imposed at the end caps, bottom and top, respectively, which are responsible for the main rotational flow perturbation here named as mechanical drive.

The operators above, $(\nabla\cdot\mathbf{V})$, ∇^2 and Δ_{visc}, are defined as

$$\nabla\cdot\mathbf{V} = \frac{1}{R}\frac{\partial}{\partial R}(RV_{\mathrm{R}}) + \frac{\partial V_Z}{\partial Z}, \tag{1w}$$

$$\nabla^2 \equiv \frac{\partial^2}{\partial Z^2} + \frac{\partial^2}{\partial R^2} + \frac{1}{R}\frac{\partial}{\partial R}, \tag{1x}$$

$$\Delta_{\mathrm{visc}} = 2\mu\left\{\left(\frac{\partial V_{\mathrm{R}}}{\partial R}\right)^2 + \left(\frac{V_{\mathrm{R}}}{R}\right)^2 + \left(\frac{\partial V_Z}{\partial Z}\right)^2 + \frac{1}{2}\left[\left(\frac{\partial V_\theta}{\partial R} - \frac{V_\theta}{R}\right)^2 + \left(\frac{\partial V_Z}{\partial R} + \frac{\partial V_{\mathrm{R}}}{\partial Z}\right)^2 + \left(\frac{\partial V_\theta}{\partial Z}\right)^2\right] - \frac{1}{3}(\nabla\cdot\mathbf{V})^2\right\}, \tag{1y}$$

where the term Δ_{visc} which appears in the energy equations refers to the viscous heat dissipation, while the term $P(\nabla\cdot\mathbf{V})$ represents the reversible work due to the compressibility.

The gas flow in ultracentrifuges is rarely solved from the above nonlinear formulation, since the secondary flow generated by the end caps' differential rotations is essentially a small perturbation to the main rotational flow due to the angular velocity Ω. The most common approach is to consider instead a linearized form of the conservation equations, obtained from the above set of equations after considering the composition of the rigid body rotation solution and the first-order perturbation solution. The rigid body rotation solution is readily

obtained considering the whole structure rotating at the same angular velocity; then, the only nonzero velocity component is the tangential one, and all the flow parameter variations in the axial direction are null. This solution is written as

$$\hat{V}_\theta(R) = \Omega R, \tag{2a}$$

$$\hat{P}(R) = P_w \ \mathrm{Exp}\left\{ \frac{G}{2}\left[\left(\frac{R}{R_2}\right)^2 - 1 \right] \right\}, \tag{2b}$$

$$\hat{\rho}(R) = \rho_w \ \mathrm{Exp}\left\{ \frac{G}{2}\left[\left(\frac{R}{R_2}\right)^2 - 1 \right] \right\}, \tag{2c}$$

where the parameter G is a velocity parameter, similar to the Mach number, defined as

$$G = \frac{M\Omega^2 R_2^2}{\Re T_0}. \tag{2d}$$

The symbol ($\hat{}$) shall represent the rigid body rotation solution. In Eqs. (2b),(2c), the subscript (w) represents the values at the outer cylinder wall, and T_0 is the gas temperature for the rigid body-type flow.

The perturbation solution is defined from small variations over the rigid body rotation solution, as

$$V_\theta(R,Z) = \Omega R + \tilde{V}_\theta(R,Z), \tag{3a}$$

$$V_R(R,Z) = 0 + \tilde{V}_R(R,Z), \tag{3b}$$

$$V_Z(R,Z) = 0 + \tilde{V}_Z(R,Z), \tag{3c}$$

$$P(R,Z) = \hat{P}(R) + \tilde{P}(R,Z), \tag{3d}$$

$$\rho(R,Z) = \hat{\rho}(R) + \tilde{\rho}(R,Z), \tag{3e}$$

$$T(R,Z) = T_0 + \tilde{T}(R,Z), \tag{3f}$$

where the symbol ($\tilde{}$) represents the perturbation dependent variables.

Substituting the above expressions into the original conservation equations (1a)–(1v), (1w)–(1y), after neglecting higher-order terms, the following linearized equations are obtained:

$$\frac{1}{R}\frac{\partial}{\partial R}(\hat{\rho}R\tilde{V}_R) + \frac{\partial}{\partial Z}(\hat{\rho}\tilde{V}_Z) = 0, \tag{4a}$$

$$-2\hat{\rho}\Omega\tilde{V}_\theta - \hat{\rho}R\Omega^2 = -\frac{\partial\tilde{P}}{\partial R} + \mu\left[\nabla^2\tilde{V}_R - \frac{\tilde{V}_R}{R^2} + \frac{1}{3}\frac{\partial}{\partial R}(\nabla\cdot\tilde{\mathbf{V}})\right], \tag{4b}$$

$$2\hat{\rho}\Omega\tilde{V}_R = \mu\left[\nabla^2\tilde{V}_\theta - \frac{\tilde{V}_\theta}{R^2}\right], \tag{4c}$$

$$\mu\left[\nabla^2\tilde{V}_Z + \frac{1}{3}\frac{\partial}{\partial Z}(\nabla\cdot\tilde{\mathbf{V}})\right] = \frac{\partial\tilde{P}}{\partial Z}, \tag{4d}$$

$$-\hat{\rho}\Omega^2 R\tilde{V}_R = k\nabla^2\tilde{T}, \tag{4e}$$

$$\frac{\tilde{P}}{\hat{P}} = \frac{\tilde{\rho}}{\hat{\rho}} + \frac{\tilde{T}}{T_0}, \tag{4f}$$

with the following boundary conditions:

$$\tilde{V}_R(R_1,Z) = 0, \tag{4g}$$

$$\tilde{V}_\theta(R_1,Z) = 0, \tag{4h}$$

$$\tilde{V}_z(R_1,Z) = 0, \tag{4i}$$

$$\tilde{T}(R_1,Z) = 0, \tag{4j}$$

$$\tilde{V}_R(R_2,Z) = 0, \tag{4k}$$

$$\tilde{V}_\theta(R_2,Z) = 0, \tag{4l}$$

$$\tilde{V}_z(R_2,Z) = 0, \tag{4m}$$

$$\tilde{T}(R_2,Z) = 0, \tag{4n}$$

$$\tilde{V}_R(R,-\tfrac{1}{2}H) = 0, \tag{4o}$$

$$\tilde{V}_\theta(R,-\tfrac{1}{2}H) = R\Delta\Omega_B, \tag{4p}$$

$$\tilde{V}_z(R,-\tfrac{1}{2}H) = 0, \tag{4q}$$

$$\tilde{T}(R,-\tfrac{1}{2}H) = 0, \tag{4r}$$

$$\tilde{V}_R(R,\tfrac{1}{2}H) = 0, \tag{4s}$$

$$\tilde{V}_\theta(R,\tfrac{1}{2}H) = R\Delta\Omega_T, \tag{4t}$$

$$\tilde{V}_z(R,\tfrac{1}{2}H) = 0, \tag{4u}$$

$$\tilde{T}(R,\tfrac{1}{2}H) = 0, \tag{4v}$$

Eqs. (4a)–(4v) for the perturbation solution are now expressed in dimensionless form by considering the following groups:

$$r = \frac{R}{R_2}, \tag{5a}$$

$$z = \frac{Z}{R_2}, \tag{5b}$$

$$v_r = \frac{\tilde{V}_R}{\Omega R_2}, \tag{5c}$$

$$v_\theta = \frac{\tilde{V}_\theta}{\Omega R_2}, \tag{5d}$$

$$v_z = \frac{\tilde{V}_Z}{\Omega R_2}, \tag{5e}$$

$$p = \frac{\tilde{P}}{P_w}, \tag{5f}$$

$$\rho = \frac{\tilde{\rho}}{\rho_w}, \tag{5g}$$

$$\Theta = \frac{\tilde{T}}{T_0}, \tag{5h}$$

$$h = \frac{H}{R_2}, \tag{5i}$$

where h is the centrifuge aspect ratio, and the dimensionless linearized system is written as

$$\frac{1}{r}\frac{\partial}{\partial r}(rv_r)+\frac{\partial v_z}{\partial z}=-Grv_r, \tag{6a}$$

$$-2v_\theta+r\Theta=-\frac{1}{G}\frac{\partial p}{\partial r}+\left(\frac{Ek}{\epsilon}\right)\times\left[\nabla^2 v_r-\frac{v_r}{r^2}+\frac{1}{3}\frac{\partial}{\partial r}(\nabla\cdot\mathbf{v})\right], \tag{6b}$$

$$2v_r=\left(\frac{Ek}{\epsilon}\right)\left[\nabla^2 v_\theta-\frac{v_\theta}{r^2}\right], \tag{6c}$$

$$\frac{1}{G}\frac{\partial p}{\partial z}=\left(\frac{Ek}{\epsilon}\right)\left[\nabla^2 v_z+\frac{1}{3}\frac{\partial}{\partial z}(\nabla\cdot\mathbf{v})\right], \tag{6d}$$

$$-Br\,rv_r=\left(\frac{Ek}{\epsilon}\right)\nabla^2\Theta, \tag{6e}$$

$$p=\rho+\Theta \tag{6f}$$

with the dimensionless boundary conditions

$$v_r(\kappa,z)=0, \tag{6g}$$
$$v_\theta(\kappa,z)=0, \tag{6h}$$
$$v_z(\kappa,z)=0, \tag{6i}$$
$$\Theta(\kappa,z)=0, \tag{6j}$$
$$v_r(1,z)=0, \tag{6k}$$
$$v_\theta(1,z)=0, \tag{6l}$$
$$v_z(1,z)=0, \tag{6m}$$
$$\Theta(1,z)=0, \tag{6n}$$
$$v_r(r,-\tfrac{1}{2}h)=0, \tag{6o}$$
$$v_\theta(r,-\tfrac{1}{2}h)=\tfrac{1}{2}r, \tag{6p}$$
$$v_z(r,-\tfrac{1}{2}h)=0, \tag{6q}$$
$$\Theta(r,-\tfrac{1}{2}h)=0, \tag{6r}$$
$$v_r(r,\tfrac{1}{2}h)=0, \tag{6s}$$
$$v_\theta(r,\tfrac{1}{2}h)=-\tfrac{1}{2}r, \tag{6t}$$
$$v_z(r,\tfrac{1}{2}h)=0, \tag{6u}$$
$$\Theta(r,\tfrac{1}{2}h)=0. \tag{6v}$$

The following characteristic dimensionless numbers, Ekman, Prandtl and Brinkman numbers, respectively, are also obtained from the above formulation:

$$Ek=\frac{\mu}{\rho_w\Omega R_2^2}, \tag{6w}$$

$$Pr=\frac{\mu c_p}{k}, \tag{6x}$$

$$Br=G\,Pr\left(\frac{\gamma-1}{\gamma}\right), \tag{6y}$$

where $\gamma=c_p/c_v$ and the quantity $\epsilon(r)$ is given by

$$\epsilon(r)=\exp\left[\frac{G}{2}(r^2-1)\right]. \tag{6z}$$

3. The streamfunction-only representation

As in previous developments with the GITT for the Navier–Stokes equations [16–21], the streamfunction-only formulation is in general preferred, due to the enhanced convergence characteristics achievable under the related eigenfunctions basis. The following expressions are here employed to define the streamfunction in terms of the velocity components:

$$v_r(r,z)=-\frac{1}{r\epsilon(r)}\frac{\partial\psi(r,z)}{\partial z}, \tag{7a}$$

$$v_z(r,z)=\frac{1}{r\epsilon(r)}\frac{\partial\psi(r,z)}{\partial r}. \tag{7b}$$

With this definition, the continuity Eq. (6a) is automatically satisfied, and Eqs. (7a) and (7b) are now applied to the remaining linearized conservation equations, resulting in the cancellation of the pressure terms in the momentum component equations. This procedure was performed through symbolic computation with the aid of the *Mathematica* system [22]. The resulting partial differential system is given by

$$E^4\psi=\left(2G^3r^3-G^2r+\frac{2G}{r}\right)\frac{\partial\psi}{\partial r}+4Gr\frac{\partial^2\psi}{\partial r\partial z^2}-\left(5G^2r^2+2G\right)\frac{\partial^2\psi}{\partial r^2}+4Gr\frac{\partial^3\psi}{\partial r^3}-\frac{2}{3}G^2r^2\times\frac{\partial^2\psi}{\partial z^2}+\frac{\epsilon^2}{Ek}\left(2r\frac{\partial v_\theta}{\partial z}-r^2\frac{\partial\Theta}{\partial z}\right), \tag{8a}$$

$$\frac{\partial^2 v_\theta}{\partial z^2}+\frac{1}{r}\frac{\partial}{\partial r}\left(r\frac{\partial v_\theta}{\partial r}\right)-\frac{v_\theta}{r^2}=-\frac{2}{Ek}\frac{\partial\psi}{\partial z}, \tag{8b}$$

$$\frac{\partial^2\Theta}{\partial z^2}+\frac{1}{r}\frac{\partial}{\partial r}\left(r\frac{\partial\Theta}{\partial r}\right)=\frac{Br}{Ek}\frac{\partial\psi}{\partial z} \tag{8c}$$

with the boundary conditions

$$\psi(\kappa,z)=0, \tag{8d}$$
$$\left.\frac{\partial\psi(r,z)}{\partial r}\right|_{r=\kappa}=0, \tag{8e}$$
$$v_\theta(\kappa,z)=0, \tag{8f}$$
$$\Theta(\kappa,z)=0, \tag{8g}$$
$$\psi(1,z)=0, \tag{8h}$$
$$\left.\frac{\partial\psi(r,z)}{\partial r}\right|_{r=1}=0, \tag{8i}$$
$$v_\theta(1,z)=0, \tag{8j}$$
$$\Theta(1,z)=0, \tag{8k}$$
$$\psi(r,-\tfrac{1}{2}h)=0, \tag{8l}$$
$$\left.\frac{\partial\psi(r,z)}{\partial z}\right|_{z=-\frac{1}{2}h}=0, \tag{8m}$$
$$v_\theta(r,-\tfrac{1}{2}h)=\tfrac{1}{2}r, \tag{8n}$$
$$\Theta(r,-\tfrac{1}{2}h)=0, \tag{8o}$$

$$\psi(r,\tfrac{1}{2}h)=0, \tag{8p}$$

$$\left.\frac{\partial\psi(r,z)}{\partial z}\right|_{z=\frac{1}{2}h}=0, \tag{8q}$$

$$v_\theta(r,\tfrac{1}{2}h)=-\tfrac{1}{2}r, \tag{8r}$$

$$\Theta(r,\tfrac{1}{2}h)=0, \tag{8s}$$

where the operators E^2 and E^4 are given, respectively, by

$$E^2\equiv\frac{\partial^2}{\partial r^2}-\frac{1}{r}\frac{\partial}{\partial r}+\frac{\partial^2}{\partial z^2}, \tag{8t}$$

$$E^4\psi=E^2(E^2\psi). \tag{8u}$$

4. Integral transformation methodology

Following the ideas in the GITT, we first select the eigenvalue problems to be used as a basis for the expansions to be proposed. The radial direction was selected for elimination through integral transformation, and three eigenvalue problems are required, for each of the dependent variables to be expanded: streamfunction, tangential velocity, and temperature.

The streamfunction eigenvalue problem, extracted from [23] and previously employed in [18,19], is given by

$$\left(\frac{\mathrm{d}^2}{\mathrm{d}r^2}+\frac{1}{r}\frac{\mathrm{d}}{\mathrm{d}r}\right)^2\mathrm{X}_i(r)=\alpha_i^4\mathrm{X}_i(r) \quad \text{for } \kappa<r<1 \text{ and } i=1,2,3,\ldots \tag{9a}$$

with boundary conditions

$$\mathrm{X}_i=0, \quad \text{in } r=\kappa, \tag{9b}$$

$$\frac{\mathrm{d}X_i}{\mathrm{d}r}=0, \quad \text{in } r=\kappa, \tag{9c}$$

$$\mathrm{X}_i=0, \quad \text{in } r=1, \tag{9d}$$

$$\frac{\mathrm{d}X_i}{\mathrm{d}r}=0, \quad \text{in } r=1, \tag{9e}$$

where $\mathrm{X}_i(r)$ and α_i represent the eigenfunctions and eigenvalues, respectively, and these solutions are obtained in normalized form as

$$\mathrm{X}_i(r)=A_{1i}J_0(\alpha_i r)+A_{2i}Y_0(\alpha_i r)+A_{3i}\frac{I_0(\alpha_i r)}{I_0(\alpha_i)}+A_{4i}\times\frac{K_0(\alpha_i r)}{K_0(\alpha_i\kappa)} \quad \text{with } i=1,2,3,\ldots \tag{9f}$$

The eigenvalues α_i's are obtained from substitution of the above solution into the boundary conditions, to yield the following algebraic system:

$$\sum_{j=1}^{4}S_{jk}A_{kj}=0, \quad k=1,\ldots,4, \tag{9g}$$

where the coefficient matrix $\mathbf{S}$ is given as

$$\mathbf{S}=\begin{bmatrix} J_0(\alpha_i\kappa) & Y_0(\alpha_i\kappa) & \frac{I_0(\alpha_i\kappa)}{I_0(\alpha_i)} & 1.0 \\ J_0(\alpha_i) & Y_0(\alpha_i) & 1.0 & \frac{K_0(\alpha_i)}{K_0(\alpha_i\kappa)} \\ -J_1(\alpha_i\kappa) & -Y_1(\alpha_i\kappa) & \frac{I_1(\alpha_i\kappa)}{I_0(\alpha_i)} & -\frac{K_1(\alpha_i\kappa)}{K_0(\alpha_i\kappa)} \\ -J_1(\alpha_i) & -Y_1(\alpha_i) & \frac{I_1(\alpha_i)}{I_0(\alpha_i)} & -\frac{K_1(\alpha_i)}{K_0(\alpha_i\kappa)} \end{bmatrix} \tag{9h}$$

and finally requiring the existence of nontrivial solutions

$$\det|\mathbf{S}|=0, \tag{9i}$$

which yields the transcendental equation for the eigenvalues α_is, while the coefficients A_{1i}, A_{2i}, A_{3i}, and A_{4i} are determined from Eq. (9g) starting with $A_{1i}=1$, for convenience.

The eigenfunctions $\mathrm{X}_i(r)$ obey the following orthogonality property:

$$\int_\kappa^1 r\mathrm{X}_i(r)\mathrm{X}_j(r)\mathrm{d}r=\begin{cases}0, & i\neq j,\\ N_{\mathrm{X}_i}(\alpha_i), & i=j,\end{cases} \tag{9j}$$

where $N_{\mathrm{X}_i}(\alpha_i)$ represent the norms of the eigenfunctions $\mathrm{X}_i(r)$ and may be analytically determined to yield

$$N_{\mathrm{X}_i}(\alpha_i)=[J_0(\alpha_i)+A_{2i}Y_0(\alpha_i)]^2-\kappa^2[J_0(\alpha_i\kappa)+A_{2i}Y_0(\alpha_i\kappa)]^2. \tag{9k}$$

The eigenvalue problem selected for the tangential velocity integral transformation is written as

$$\frac{1}{r}\frac{\mathrm{d}}{\mathrm{d}r}\left[r\frac{\mathrm{d}\Gamma_m(r)}{\mathrm{d}r}\right]+\left(\beta_m^2-\frac{1}{r^2}\right)\Gamma_m(r)=0 \quad \text{with } m=1,2,3,\ldots \tag{10a}$$

with boundary conditions

$$\Gamma_m(\kappa)=0, \tag{10b}$$

$$\Gamma_m(1)=0, \tag{10c}$$

and its solution is readily given by

$$\Gamma_m(r)=J_1(\beta_m r)Y_1(\beta_m)-J_1(\beta_m)Y_1(\beta_m r) \tag{10d}$$

while the eigenvalues are evaluated from

$$J_1(\beta_m\kappa)Y_1(\beta_m)-J_1(\beta_m)Y_1(\beta_m\kappa)=0. \tag{10e}$$

The eigenfunctions Γ_m (r) follow the orthogonality property

$$\int_\kappa^1 r\Gamma_m(r)\Gamma_l(r)\mathrm{d}r=\begin{cases}0 & \text{for } m\neq l,\\ N_{\Gamma_m}(\beta_m) & \text{for } m=l,\end{cases} \tag{10f}$$

where the norms of eigenfunctions Γ_m (r) are writen as

$$N_{\Gamma_m}(\beta_m)=\frac{2}{\pi^2}\frac{J_1^2(\beta_m\kappa)-J_1^2(\beta_m)}{\beta_m^2J_1^2(\beta_m\kappa)}. \tag{10g}$$

For the temperature field, we have taken the eigenvalue problem below

$$\frac{1}{r}\frac{\mathrm{d}}{\mathrm{d}r}\left[r\frac{\mathrm{d}\Phi_n(r)}{\mathrm{d}r}\right]+\lambda_n^2\Phi_n(r)=0 \quad \text{with } n=1,2,3,\ldots \tag{11a}$$

with boundary conditions

$$\Phi_n(\kappa)=0, \tag{11b}$$

$$\Phi_n(1)=0 \tag{11c}$$

again readily solved as

$$\Phi_n(r)=J_0(\lambda_n r)Y_0(\lambda_n)-J_0(\lambda_n)Y_0(\lambda_n r) \tag{11d}$$

and the transcendental equation for the eigenvalues

$$J_0(\lambda_n\kappa)Y_0(\lambda_n)-J_0(\lambda_n)Y_0(\lambda_n\kappa)=0. \tag{11e}$$

The eigenfunctions $\Phi_n(r)$ obey the orthogonality property

$$\int_\kappa^1 r\Phi_n(r)\Phi_k(r)\mathrm{d}r=\begin{cases}0 & \text{for } n\neq k,\\ N_{\Phi_n}(\lambda_n) & \text{for } n=k\end{cases} \tag{11f}$$

with the norms given by the analytical expression

$$N_{\Phi_n}(\lambda_n)=\frac{2}{\pi^2}\frac{J_0^2(\lambda_n\kappa)-J_0^2(\lambda_n)}{\lambda_n^2J_0^2(\lambda_n\kappa)}. \tag{11g}$$

Employing the above orthogonality properties, the following integral transform pairs are constructed:

Streamfunction:

$$\bar{\psi}_i(z)=\int_\kappa^1 r\tilde{\mathrm{X}}_i(r)\psi(r,z)\mathrm{d}r \quad \text{(transform)}, \tag{12a}$$

$$\psi(r,z)=\sum_{i=1}^{\infty}\tilde{\mathrm{X}}_i(r)\bar{\psi}_i(z) \quad \text{(inverse)}. \tag{12b}$$

Tangential velocity component:

$$\bar{v}_m(z)=\int_\kappa^1 r\tilde{\Gamma}_m(r)v_\theta(r,z)\mathrm{d}r \quad \text{(transform)}, \tag{13a}$$

$$v_\theta(r,z)=\sum_{m=1}^{\infty}\tilde{\Gamma}_m(r)\bar{v}_m(z) \quad \text{(inverse)}. \tag{13b}$$

Temperature:

$$\bar{\Theta}_n(z)=\int_\kappa^1 r\tilde{\Phi}_n(r)\Theta(r,z)\mathrm{d}r \quad \text{(transform)}, \tag{14a}$$

$$\Theta(r,z)=\sum_{n=1}^{\infty}\tilde{\Phi}_n(r)\bar{\Theta}_n(z) \quad \text{(inverse)}, \tag{14b}$$

and the following normalized eigenfunctions were defined:

$$\tilde{\mathrm{X}}_i(r)=\frac{\mathrm{X}_i(r)}{\sqrt{N_{\mathrm{X}_i}(\alpha_i)}}, \tag{15a}$$

$$\tilde{\Gamma}_m(r)=\frac{\Gamma_m(r)}{\sqrt{N_{\Gamma_m}(\beta_m)}}, \tag{15b}$$

$$\tilde{\Phi}_n(r)=\frac{\Phi_n(r)}{\sqrt{N_{\Phi_n}(\lambda_n)}}. \tag{15c}$$

Operating Eqs. (8a)–(8c) with $\int_\kappa^1 r\tilde{\mathrm{X}}_i(r)\mathrm{d}r$, $\int_\kappa^1 r\tilde{\Gamma}_m(r)\mathrm{d}r$ and $\int_\kappa^1 r\tilde{\Phi}_n(r)\mathrm{d}r$, respectively, the following coupled ordinary differential system results:

$$\frac{\mathrm{d}^4\bar{\psi}_i}{\mathrm{d}z^4}(z)=-\alpha_i^4\bar{\psi}_i(z)+\sum_{j=1}^{\infty}\left[A_{ij}\bar{\psi}_j(z)+B_{ij}\frac{\mathrm{d}^2\bar{\psi}_i(z)}{\mathrm{d}z^2}\right]+\frac{2}{Ek}\sum_{m=1}^{\infty}C_{im}\frac{\mathrm{d}\bar{v}_m(z)}{\mathrm{d}z}-\frac{1}{Ek}\sum_{n=1}^{\infty}D_{in}\frac{\mathrm{d}\bar{\Theta}_n(z)}{\mathrm{d}z}, \tag{16a}$$

$$\frac{\mathrm{d}^2\bar{v}_m}{\mathrm{d}z^2}(z)=\beta_m^2\bar{v}_m(z)-\frac{2}{Ek}\left[\sum_{j=1}^{\infty}E_{mj}\frac{\mathrm{d}\bar{\psi}_j(z)}{\mathrm{d}z}\right], \tag{16b}$$

$$\frac{\mathrm{d}^2\bar{\Theta}_n}{\mathrm{d}z^2}(z)=\lambda_n^2\bar{\Theta}_n(z)+\frac{Br}{Ek}\left[\sum_{j=1}^{\infty}F_{nj}\frac{\mathrm{d}\bar{\psi}_j(z)}{\mathrm{d}z}\right]. \tag{16c}$$

Similarly proceeding with the integral transformation of the boundary conditions, Eqs. (8l)–(8s), one finds

$$\bar{\psi}_i(-\tfrac{1}{2}h)=0, \tag{16d}$$

$$\bar{\psi}_i'(-\tfrac{1}{2}h)=0, \tag{16e}$$

$$\bar{v}_m(-\tfrac{1}{2}h)=\tfrac{1}{2}f_m, \tag{16f}$$

$$\bar{\Theta}_n(-\tfrac{1}{2}h)=0, \tag{16g}$$

$$\bar{\psi}_i(\tfrac{1}{2}h)=0, \tag{16h}$$

$$\bar{\psi}_i'(\tfrac{1}{2}h)=0, \tag{16i}$$

$$\bar{v}_m(\tfrac{1}{2}h)=-\tfrac{1}{2}f_m, \tag{16j}$$

$$\bar{\Theta}_n(\tfrac{1}{2}h)=0, \tag{16k}$$

where the integral coefficients that appear in the infinite ODE system for the transformed potentials are given by

$$A_{ij}=\int_\kappa^1\tilde{\mathrm{X}}_i(r)\left[(4+4Gr^2)\tilde{\mathrm{X}}_j'''(r)+\left(5G^2r^3+2Gr-\frac{4}{r^2}\right)\tilde{\mathrm{X}}_j''(r)+\left(2G^3r^4-G^2r^2+2G+\frac{4}{r^2}\right)\tilde{\mathrm{X}}_j'(r)\right]\mathrm{d}r, \tag{17a}$$

$$B_{ij}=\int_\kappa^1\tilde{\mathrm{X}}_i(r)\left[(2+4Gr^2)\tilde{\mathrm{X}}_j'(r)-2r\tilde{\mathrm{X}}_j''(r)-\frac{2}{3}G^2r^3\tilde{\mathrm{X}}_j(r)\right]\mathrm{d}r, \tag{17b}$$

$$C_{im}=\int_\kappa^1 r^2\epsilon(r)^2\tilde{\mathrm{X}}_i(r)\tilde{\Gamma}_m(r)\mathrm{d}r, \tag{17c}$$

$$D_{in}=\int_\kappa^1 r^3\epsilon(r)^2\tilde{\mathrm{X}}_i(r)\tilde{\Phi}_n(r)\mathrm{d}r, \tag{17d}$$

$$E_{mj}=\int_\kappa^1\tilde{\Gamma}_m(r)\tilde{\mathrm{X}}_j(r)\mathrm{d}r, \tag{17e}$$

$$F_{nj}=\int_\kappa^1 r\tilde{\Phi}_n(r)\tilde{\mathrm{X}}_j(r)\mathrm{d}r, \tag{17f}$$

$$f_m=\int_\kappa^1 r^2\tilde{\Gamma}_m(r)\mathrm{d}r. \tag{17g}$$

5. Computational procedure

The above ODE system, although coupled and infinite, is still linear and homogeneous. Therefore, its analytical solution may be obtained from the appropriate matrix eigensystem analysis. For this purpose, system (16a)–(16c) is rewritten as a first-order system in the form

$$\bar{Y}_i(z) = \bar{\psi}_i(z), \tag{18a}$$

$$\bar{Y}_{i+NT}(z) = \frac{\mathrm{d}\bar{\psi}_i(z)}{\mathrm{d}z}, \tag{18b}$$

$$\bar{Y}_{i+2NT}(z) = \frac{\mathrm{d}^2\bar{\psi}_i(z)}{\mathrm{d}z^2}, \tag{18c}$$

$$\bar{Y}_{i+3NT}(z) = \frac{\mathrm{d}^3\bar{\psi}_i(z)}{\mathrm{d}z^3}, \tag{18d}$$

$$\begin{aligned}\frac{\mathrm{d}\bar{Y}_{i+3NT}(z)}{\mathrm{d}z} &= \frac{\mathrm{d}^4\bar{\psi}_i(z)}{\mathrm{d}z^4}\\ &= -\alpha_i^4\bar{Y}_i(z) + \sum_{j=1}^{\infty}\left[A_{ij}\bar{Y}_j(z) + B_{ij}\bar{Y}_{j+2NT}(z)\right]\\ &\quad + \frac{1}{Ek}\left[\sum_{m=1}^{\infty}2C_{im}\bar{Y}_{m+5NT}(z) - \sum_{n=1}^{\infty}D_{in}\bar{Y}_{n+7NT}(z)\right],\end{aligned} \tag{18e}$$

$$\bar{Y}_{m+4NT}(z) = \bar{v}_m(z), \tag{18f}$$

$$\bar{Y}_{m+5NT}(z) = \frac{\mathrm{d}\bar{v}_m(z)}{\mathrm{d}z}, \tag{18g}$$

$$\begin{aligned}\frac{\mathrm{d}\bar{Y}_{m+5NT}(z)}{\mathrm{d}z} &= \frac{\mathrm{d}^2\bar{v}_m(z)}{\mathrm{d}z^2}\\ &= \beta_m^2\bar{Y}_{m+4NT}(z) - \frac{2}{Ek}\left[\sum_{j=1}^{\infty}E_{mj}\bar{Y}_{j+NT}\right],\end{aligned} \tag{18h}$$

$$\bar{Y}_{n+6NT}(z) = \bar{\Theta}_n(z), \tag{18i}$$

$$\bar{Y}_{n+7NT}(z) = \frac{\mathrm{d}\bar{\Theta}_n(z)}{\mathrm{d}z}, \tag{18j}$$

$$\begin{aligned}\frac{\mathrm{d}\bar{Y}_{n+7NT}(z)}{\mathrm{d}z} &= \frac{\mathrm{d}^2\bar{\Theta}_n(z)}{\mathrm{d}z^2}\\ &= \lambda_n^2\bar{Y}_{n+6NT}(z) + \frac{Br}{Ek}\left[\sum_{j=1}^{\infty}F_{nj}\bar{Y}_{j+NT}(z)\right],\end{aligned} \tag{18k}$$

while the boundary conditions are rewritten as

$$\bar{Y}_i(-\tfrac{1}{2}h) = 0, \tag{18l}$$

$$\bar{Y}_{i+NT}(-\tfrac{1}{2}h) = 0, \tag{18m}$$

$$\bar{Y}_{m+4NT}(-\tfrac{1}{2}h) = \tfrac{1}{2}f_m, \tag{18n}$$

$$\bar{Y}_{n+6NT}(-\tfrac{1}{2}h) = 0, \tag{18o}$$

$$\bar{Y}_i(\tfrac{1}{2}h) = 0, \tag{18p}$$

$$\bar{Y}_{i+NT}(\tfrac{1}{2}h) = 0, \tag{18q}$$

$$\bar{Y}_{m+4NT}(\tfrac{1}{2}h) = -\tfrac{1}{2}f_m, \tag{18r}$$

$$\bar{Y}_{n+6NT}(\tfrac{1}{2}h) = 0. \tag{18s}$$

The infinite series in each equation, for computational purposes, were truncated to a sufficiently large finite order NT, here taken as equal for each potential so as to simplify the convergence analysis. For optimum computational behavior, there should be no difficulty in accounting for variable truncation orders among the potentials. In the present choice, the first terms of order $1,\ldots,4NT$ represent the transformed streamfunction and its derivatives, the next $4NT+1,\ldots,6NT$ are relative to the tangential velocity and the last ones, $6NT+1,\ldots,8NT$ are associated with the temperature.

System (18a)–(18s) may be represented in matrix form as

$$\mathbf{Y}' = \mathbf{M}\mathbf{Y}, \tag{19}$$

where $\mathbf{M}$ is the coefficient matrix of order $8NT$, independent of the axial coordinate.

The solution vector $\mathbf{Y}$ may then be constructed as

$$\mathbf{Y} = \zeta \mathrm{e}^{\delta z} \tag{20}$$

and substitution of Eq. (20) into system (19) yields the matrix eigenvalue problem

$$(\mathbf{M} - \delta\mathbf{I})\zeta = 0, \tag{21}$$

where $\mathbf{I}$ is the identity matrix, δ are the eigenvalues of matrix $\mathbf{M}$ and ζ the associated eigenvectors. The final solution for the transformed potentials and their derivatives is then constructed as

$$\bar{Y}_i(z) = \sum_{j=1}^{8NT} c_j\zeta_j^i\mathrm{e}^{\delta_j z}, \quad i = 1,\ldots,8NT, \tag{22}$$

where the truncation order NT may be varied to satisfy user prescribed accuracy requirements.

The constants c_j's are obtained after substitution of the solution (22) into the boundary conditions (18l)–(18s), making $z_1 = \frac{1}{2}h$, to find:

For $z = -z_1$:

$$\begin{aligned}
&c_1\zeta_1^i\mathrm{e}^{-\delta_1 z_1} + \ldots + c_{8NT}\zeta_{8NT}^i\mathrm{e}^{-\delta_{8NT}z_1} = 0, \quad i = 1,\ldots,NT,\\
&c_1\zeta_1^i\mathrm{e}^{-\delta_1 z_1} + \ldots + c_{8NT}\zeta_{8NT}^i\mathrm{e}^{-\delta_{8NT}z_1} = 0,\\
&\quad i = NT+1,\ldots,2NT,\\
&c_1\zeta_1^i\mathrm{e}^{-\delta_1 z_1} + \ldots + c_{8NT}\zeta_{8NT}^i\mathrm{e}^{-\delta_{8NT}z_1} = \frac{1}{2}f_m,\\
&\quad \begin{cases} i = 4NT+1,\ldots,5NT,\\ m = 1,\ldots,NT \end{cases}\\
&c_1\zeta_1^i\mathrm{e}^{-\delta_1 z_1} + \ldots + c_{8NT}\zeta_{8NT}^i\mathrm{e}^{-\delta_{8NT}z_1} = 0,\\
&\quad i = 6NT+1,\ldots,7NT.
\end{aligned} \tag{23a}$$

For $z = z_1$:

$$
\begin{aligned}
&c_1\zeta_1^i e^{\delta_1 z_1} + \ldots + c_{8NT}\zeta_{8NT}^i e^{\delta_{8NT} z_1} = 0, \quad i = 1, \ldots, NT,\\
&c_1\zeta_1^i e^{\delta_1 z_1} + \ldots + c_{8NT}\zeta_{8NT}^i e^{\delta_{8NT} z_1} = 0,\\
&\quad i = NT+1, \ldots, 2NT,\\
&c_1\zeta_1^i e^{\delta_1 z_1} + \ldots + c_{8NT}\zeta_{8NT}^i e^{\delta_{8NT} z_1} = -\frac{1}{2} f_m,\\
&\quad \begin{cases} i = 4NT+1, \ldots, 5NT,\\ m = 1, \ldots, NT \end{cases}\\
&c_1\zeta_1^i e^{\delta_1 z_1} + \ldots + c_{8NT}\zeta_{8NT}^i e^{\delta_{8NT} z_1} = 0,\\
&\quad i = 6NT+1, \ldots, 7NT.
\end{aligned}
\tag{23b}
$$

For best computational performance, the constants are redefined as

$$
c_j^* = \begin{cases} c_j e^{\delta_j z_1} & \text{if } \mathrm{Real}(\delta_j) \geqslant 0,\\ c_j e^{-\delta_j z_1} & \text{if } \mathrm{Real}(\delta_j) < 0. \end{cases} \tag{24}
$$

The IMSL mathematical library [24] is employed for the accuracy controlled solution of these algebraic problems. Once the constants c_j^*'s have been numerically evaluated, the solution vector is finally reconstructed from

$$
\bar{Y}_i(z) = \sum_{j=1}^{8NT} \begin{cases} c_j^* \zeta_j^i e^{\delta_j (z - z_1)} & \\ \quad \text{if } \mathrm{Real}(\delta_j) \geqslant 0, & \\ c_j^* \zeta_j^i e^{\delta_j (z + z_1)} & \\ \quad \text{if } \mathrm{Real}(\delta_j) < 0, & \end{cases} \quad i = 1, \ldots, 8NT, \tag{25}
$$

The original potentials are then analytically obtained, at any (r, z) position within the ultracentrifuge, from the inversion formulae, Eqs. (12b), (13b) and (14b), yielding the desired final solutions for the streamfunction, tangential velocity and temperature perturbation solutions in dimensionless form.

6. Results and discussion

The numerical results here presented were obtained for the same input data as considered in [11] for covalidation purposes. Dickinson and Jones model the centrifuge as a full cylinder, without taking into account the presence of the inner feeding tube. However, it was here verified that the same physical behavior is attained within a certain range of concentric cylinder radii ratios in comparison to the full cylinder simplification, due to the strong density stratification produced by the very high rotational speeds, concentrating most of the fluid mass within a thin layer attached to the outer cylinder wall. The values employed for the dimensionless parameters are as follows:

$$
h = 30, \quad G = 35, \quad Pr\left(\frac{\gamma - 1}{\gamma}\right) = 0.06, \quad Br = 2.1,
$$

$$
\kappa = \begin{cases} 0.05 \\ 0.10 \\ 0.15 \\ 0.50 \end{cases}, \quad Ek = \begin{cases} 5.40 \times 10^{-6} \\ 2.70 \times 10^{-6} \\ 6.73 \times 10^{-7} \\ 3.37 \times 10^{-7} \\ 5.60 \times 10^{-8} \end{cases}.
$$

Table 1
Convergence behavior of the streamfunction for $Ek = 3.37 \times 10^{-7}$ and at $z = 0$

NT	$r = 0.80$ ($\psi \times 10^6$)	0.85 ($\psi \times 10^6$)	0.90 ($\psi \times 10^5$)	0.95 ($\psi \times 10^5$)	0.975 ($\psi \times 10^5$)
$\kappa = 0.10$					
300	1.092	4.686	1.870	5.325	5.143
340	1.173	4.853	1.885	5.299	5.122
360	1.194	4.896	1.889	5.292	5.116
380	1.208	4.925	1.892	5.288	5.112
400	1.218	4.946	1.893	5.284	5.110
$\kappa = 0.15$					
280	1.204	4.911	1.888	5.287	5.114
300	1.229	4.962	1.893	5.279	5.108
320	1.220	4.950	1.894	5.283	5.109
340	1.228	4.968	1.895	5.280	5.106
360	1.234	4.979	1.896	5.278	5.105
NT	$r = 0.80$ ($\psi \times 10^7$)	0.85 ($\psi \times 10^6$)	0.90 ($\psi \times 10^5$)	0.95 ($\psi \times 10^5$)	0.975 ($\psi \times 10^5$)
$\kappa = 0.50$					
100	9.207	4.291	1.815	5.349	5.188
180	9.871	4.441	1.834	5.332	5.168
240	9.886	4.444	1.834	5.331	5.167
280	9.888	4.444	1.834	5.331	5.167
300	9.889	4.444	1.834	5.331	5.167

Our initial concern was to illustrate the excellent convergence rates achieved by the present eigenfunction expansion approach, as presented in Table 1, for the streamfunction radial profile convergence behavior at the axial position $z = 0$, with different radii ratios ($\kappa = 0.1$, 0.15 and 0.50). It can be observed that convergence improves as the radii ratio is increased; for the lowest radii ratio of 0.1, full convergence to four significant digits is yet not reached for truncation orders $NT = 400$, while it is surely achieved for the other situations. For $\kappa = 0.50$, with less than 300 terms, full convergence to four significant digits is observed throughout the range of radial positions inspected. This convergence behavior is quite similar to that observed in the more straightforward forced convection application considered in [19].

In Fig. 2 we plot the streamfunction radial profiles at $z = 0$, for the four different geometric configurations ($\kappa = 0.05$, 0.10, 0.15 and 0.50) and for $Ek = 3.37\times\ 10^{-7}$. It is then evident, both from the

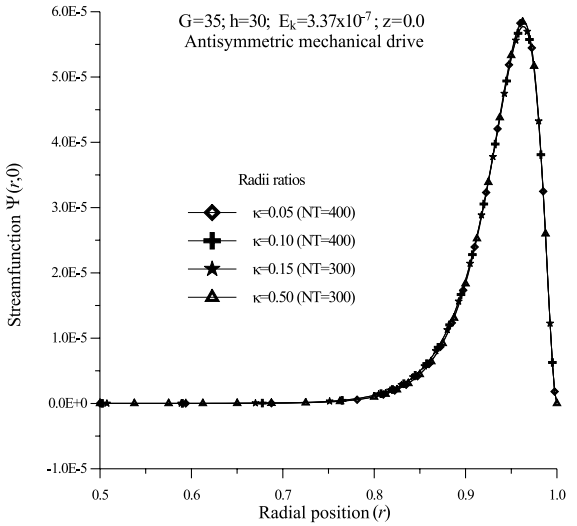

Fig. 2. Comparison of radial profiles of the streamfunction for $z = 0$, $Ek = 3.37 \times 10^{-7}$ and different radii ratios.

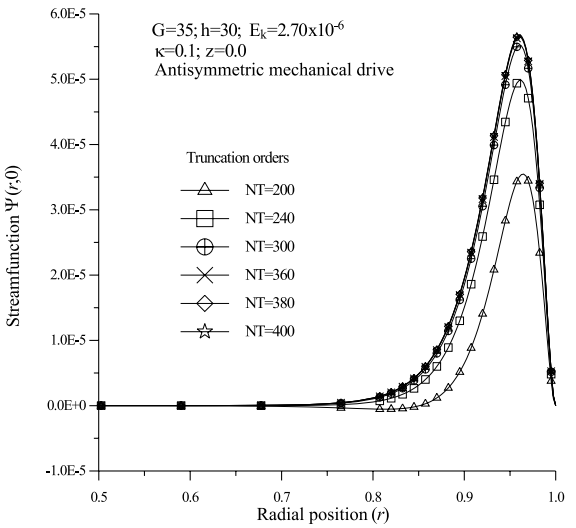

Fig. 4. Convergence behavior of radial profile of the streamfunction for $z = 0$, $Ek = 2.70 \times 10^{-6}$ and $\kappa = 0.10$.

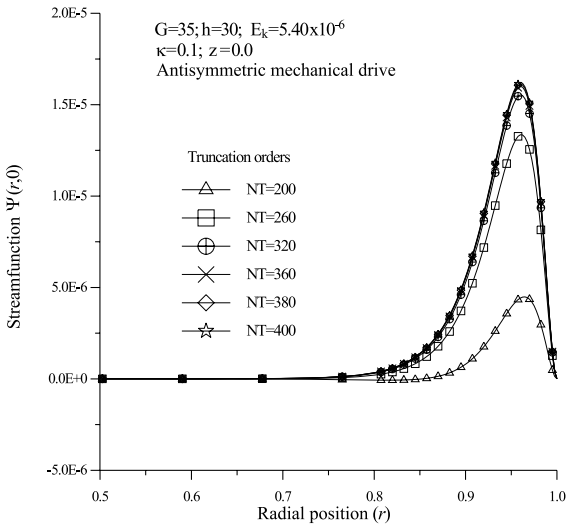

Fig. 3. Convergence behavior of radial profile of the streamfunction for $z = 0$, $Ek = 5.40 \times 10^{-6}$ and $\kappa = 0.10$.

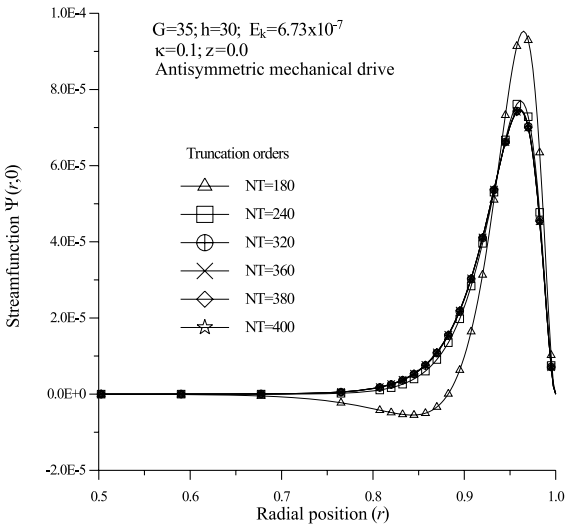

Fig. 5. Convergence behavior of radial profile of the streamfunction for $z = 0$, $Ek = 6.73 \times 10^{-7}$ and $\kappa = 0.10$.

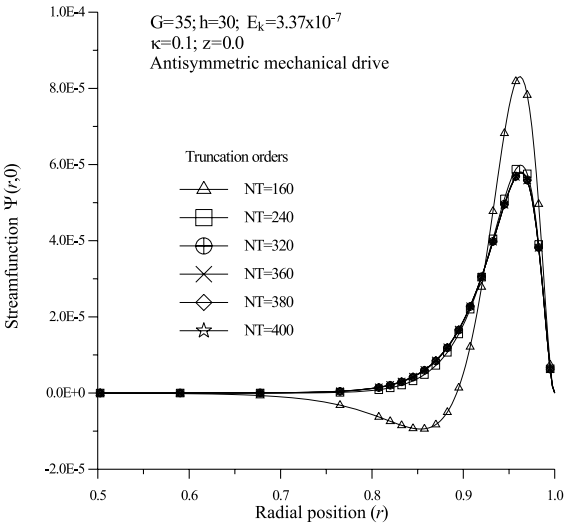

Fig. 6. Convergence behavior of radial profile of the streamfunction for $z = 0$, $Ek = 3.37 \times 10^{-7}$ and $\kappa = 0.10$.

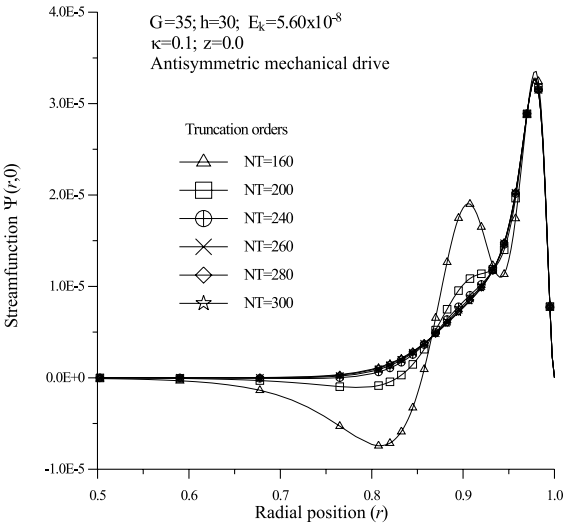

Fig. 7. Convergence behavior of radial profile of the streamfunction for $z = 0$, $Ek = 5.60 \times 10^{-8}$ and $\kappa = 0.10$.

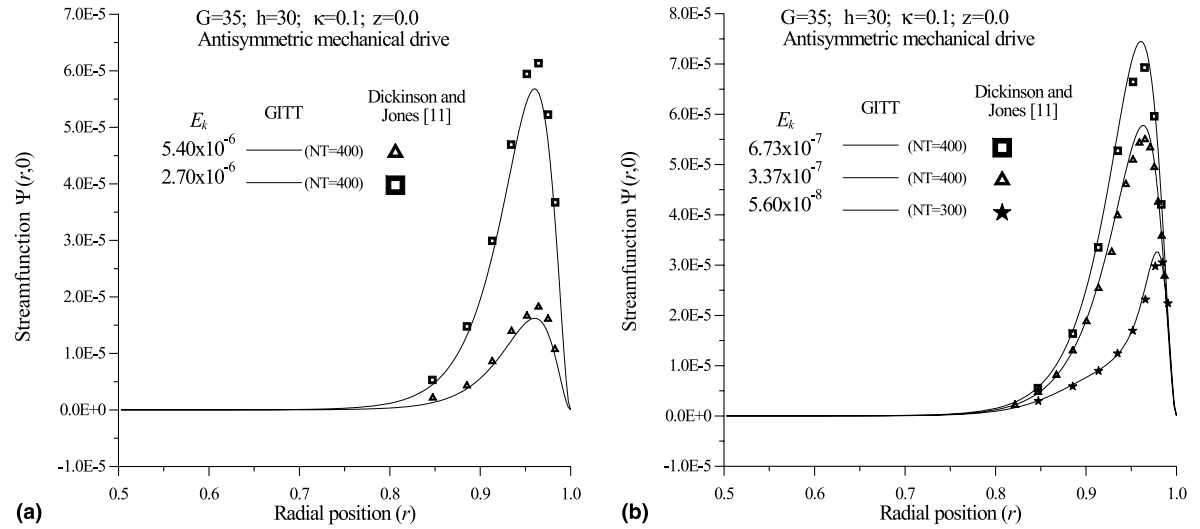

Fig. 8. Comparisons of radial profile of the streamfunction for the present GITT converged solution and finite differences solution in [11] for: (a) $Ek = 5.40 \times 10^{-6}$ and 2.7×10^{-6}; (b) $Ek = 6.73 \times 10^{-7}$, 3.37×10^{-7} and 5.60×10^{-8}.

values in Table 1 and from this figure, that at least in this radii ratios range $(0.05 \leqslant \kappa \leqslant 0.5)$, there is no significant difference in the gas flow behavior within the centrifuge, as mentioned above, and thus the exact actual boundary location for the inner cylinder does not play a major role in the final flow field simulation. It means that in this range the flow is very little perturbed by the inner boundary condition. Despite the fact that the convergence is faster for higher values of the radii ratio, the remaining of the present simulation was performed with the more actual configuration ratio of 0.1.

In Figs. 3–7 we illustrate the convergence behavior of the streamfunction radial profiles at $z = 0$ and $\kappa = 0.1$, for all the Ekman number values considered. It can be observed that for Ekman number of order 10^{-6}, shown in Figs. 3 and 4, around 360 terms were required for a full graphical coincidence among the solutions with different truncation orders, while for values of the order of 10^{-7}, the curves merging is already noticeable for about 320 terms in the expansions (Figs. 5 and 6). In the lowest value of Ekman number adopted, $Ek = 5.60 \times 10^{-8}$, 240 terms were enough to demonstrate full convergence to the graph scale, as in Fig. 7.

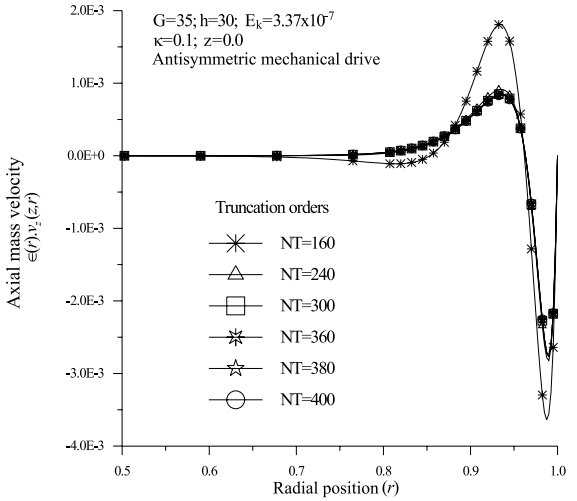

Fig. 9. Convergence behavior of the axial mass velocity for $z = 0$, $Ek = 3.37 \times 10^{-7}$ and $\kappa = 0.10$.

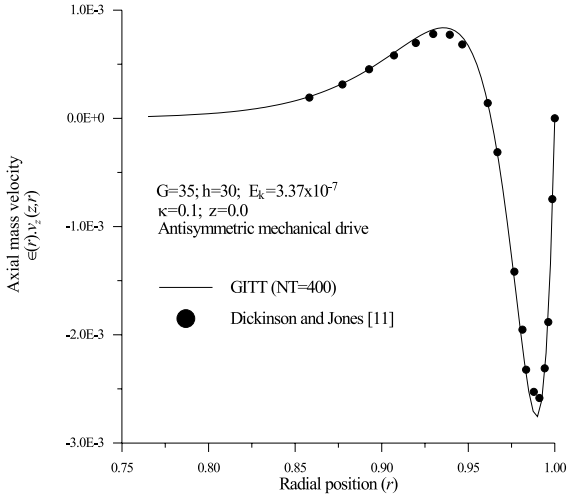

Fig. 10. Comparison of radial profile of the axial mass velocity for the present GITT converged solution and finite differences solution in [11] for $z = 0$, $Ek = 3.37 \times 10^{-7}$ and $\kappa = 0.10$.

Next, we were concerned with the co-validation of the present fully converged results against the numerical solution in [11], which is again shown in terms of the streamfunction radial profiles, within Fig. 8(a) and (b). A good agreement is observed for all the cases considered, especially close to the inner wall and at the return layer adjacent to the outer wall (Stewartson layer). Some deviations are observable at the peak regions, where flow reversal occurs, probably due to the fairly rough mesh employed in the finite differences computation of [11] around this region.

Fig. 9 presents the convergence behavior of the axial mass velocity radial profile at $z = 0$ with $Ek = 3.37 \times 10^{-7}$ and $\kappa = 0.10$. It can be said that the curves are already fully coincident for values of $NT = 300$. The flow changes direction at around $r = 0.95$, which corresponds to the maximum value of the streamfunction in Fig. 6, for the present value of Ekman number. Again, the comparison with the numerical results in [11] demonstrates the reasonably good agreement, as reproduced in Fig. 10.

Fig. 11(a)–(e) illustrate the physical nature of this compressible flow, for the various Ekman number values considered, by plotting the streamfunction isolines within the centrifuge. It is first of all interesting to notice the symmetry of the flow with respect to the plane $z = 0$, an expected behavior due to the anti-symmetric mechanical drive at the end caps, adopted for the present analysis. Also, quite noticeable is the formation of the Ekman layers adjacent to the end caps, besides the presence of the Stewartson layer adjacent to the outer cylinder wall. The Ekman layers are more clearly observed for the higher values of the Ekman number, Fig. 11(a)–(c), while the Stewartson layer is more evident in Fig. 11(d) and (e), at the lower values of Ekman number, due to the increased importance of the centrifugal forces.

7. Conclusions

The GITT was successfully employed in the simulation of compressible flow within rapidly rotating concentric cylinders, as required for the accurate representation of gas flow fields within ultracentrifuges for isotopic separation. A formal analytical solution was developed and accurate results were obtained for various physical situations, and employed in the co-validation with previously reported purely numerical solutions for the case of an anti-symmetric mechanical drive, with very good overall agreement. The analytical nature of the proposed solution is particularly attractive in terms of computational performance when applied to the optimization of the centrifugation and separation parameters, in connection with the radioisotopes concentration field determination. All the results here reported were obtained within mild computational effort on personal microcomputers.

Acknowledgements

The authors would like to acknowledge the partial financial support provided by Brazilian Navy Technology Center, FAPERJ, PRONEX and CNPq, all of them sponsoring agencies in Brazil.

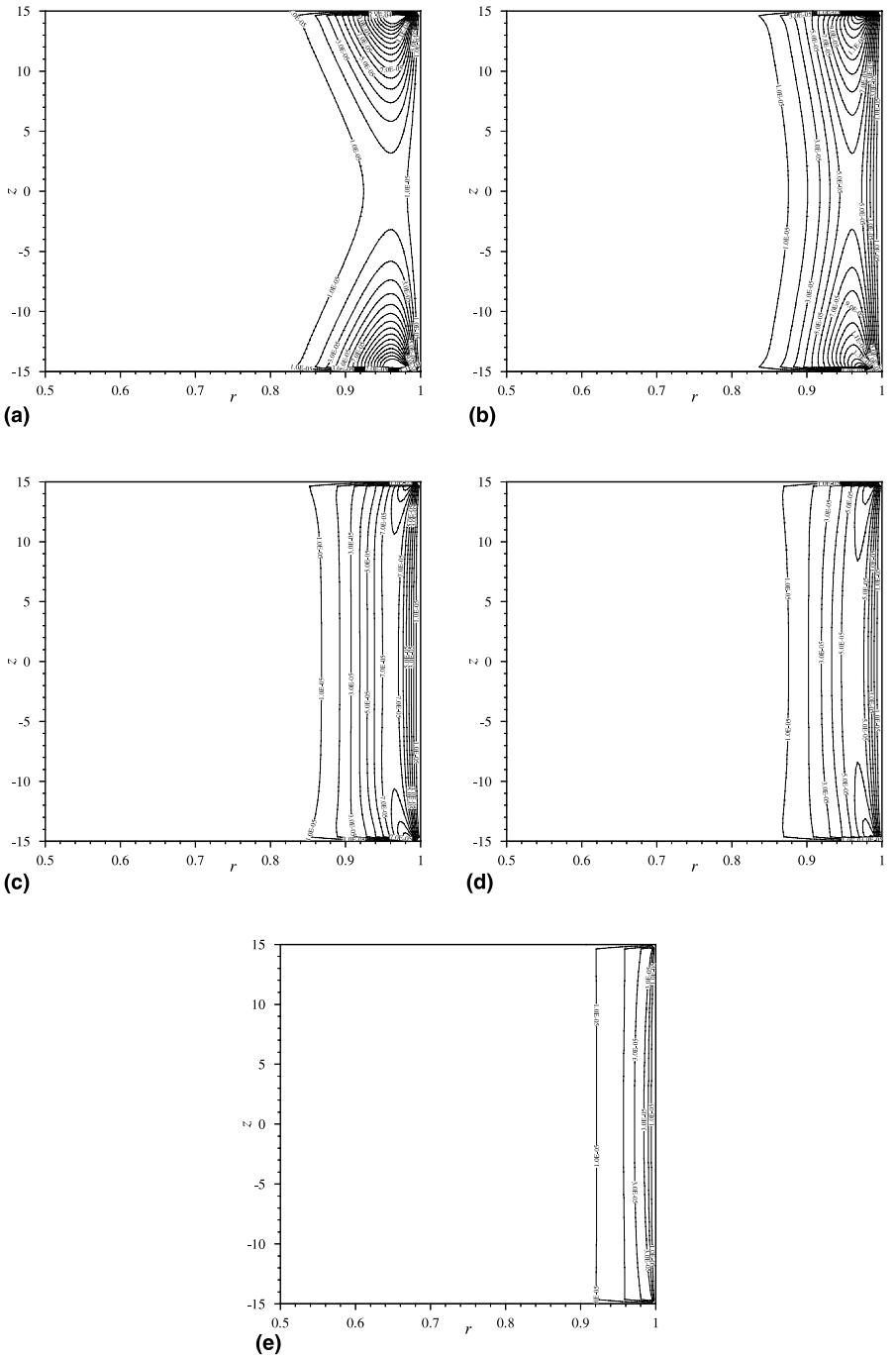

Fig. 11. Isolines of streamfunction for anti-symmetric mechanical drive for $h = 30$, $G = 35$ and $\kappa = 0.10$, for: (a) $Ek = 5.40 \times 10^{-6}$; (b) $Ek = 2.70 \times 10^{-6}$; (c) $Ek = 6.73 \times 10^{-7}$; (d) $Ek = 3.37 \times 10^{-7}$ and (e) $Ek = 5.60 \times 10^{-8}$.

References

[1] Soubbaramayer, Centrifugation, in: S. Villani (Ed.), Uranium Enrichment, Topics in Applied Physics, vol. 35, 1979, pp. 183–244.

[2] R.M. Cotta, Integral Transforms in Computational Heat and Fluid Flow, CRC Press, Boca Raton, FL, 1993.

[3] R.M. Cotta, M.D. Mikhailov, Heat Conduction – Lumped Analysis, Integral Transforms, Symbolic Computation, Wiley, Chichester, UK, 1997.

[4] R.M. Cotta, The Integral Transform Method in Thermal & Fluids Sciences & Engineering, Begell House, New York, 1998.
[5] R.M. Cotta, Benchmark results in computational heat and fluid flow: The integral transform method, Int. J. Heat Mass Transfer (Invited Paper) 37 (Suppl. 1) (1994) 381–394.
[6] W. Nakayama, S. Usui, Flow in rotating cylinder of a gas centrifuge, J. Nucl. Sci. Technol. 11 (6) (1974) 242–262.
[7] T. Sakurai, T. Matsuda, Gasdynamics of a centrifugal machine, J. Fluid Mech. 62 (4) (1974) 727–736.
[8] J.P. Lahargue, Soubbaramayer, A numerical model for the investigation of the flow and isotope concentration field in an ultracentrifuge, Comput. Meth. Appl. Mech. Eng. 15 (1978) 259–273.
[9] Soubbaramayer, J. Billet, A numerical method for optimizing the gas flow field in a centrifuge, Comput. Meth. Appl. Mech. Eng. 24 (1980) 165–185.
[10] H.G. Wood, J.B. Morton, Onsager's Pancake approximation for the fluid dynamics of a gas centrifuge, J. Fluid Mech. 101 (1) (1980) 1–31.
[11] G.J. Dickinson, I.P. Jones, Numerical solutions for the compressible flow in a rapidly rotating cylinder, J. Fluid Mech. 107 (1981) 89–107.
[12] D. Gunzburger, H.G. Wood, A finite element method for the onsager pancake equation, Comput. Meth. Appl. Mech. Eng. 31 (1982) 43–59.
[13] H.G. Wood, G. Sanders, Rotating compressible flows with internal sources and sinks, J. Fluid Mech. 127 (1983) 299–313.
[14] H.G. Wood, J.A. Jordan, M.D. Gunzburger, The effects of curvature on the flow field in rapidly rotating gas centrifuge, J. Fluid Mech. 140 (1984) 373–395.
[15] Z. Cunzhen, A.T. Conlisk, Separation in a gas centrifuge at high feed flow rate, J. Fluid Mech. 208 (1989) 355–373.
[16] J.S. Perez Guerrero, R.M. Cotta, Integral transform method for Navier–Stokes equations in stream function-only formulation, Int. J. Numer. Meth. Fluids 15 (1992) 399–409.
[17] J.S. Perez Guerrero, R.M. Cotta, Benchmark integral transform results for flow over a backward-facing step, Comput. Fluids 25 (5) (1996) 527–540.
[18] L.M. Pereira, J.S. Perez Guerrero, R.M. Cotta, Integral transformation of the Navier–Stokes equations in cylindrical geometry, Comput. Mech. 21 (1) (1998) 60–70.
[19] L.M. Pereira, R.M. Cotta, J.S. Perez Guerrero, Analysis of laminar forced convection in annular ducts using integral transforms, in: Proceedings of the 15th Brazilian Congress of Mechanical Engineering, COBEM 99, Águas de Lindóia, São Paulo, Brazil, December 1999 (CD-ROM); also, Hybrid Meth. Eng., 2(2) (2000) 221–232.
[20] M.A. Leal, J.S. Perez Guerrero, R.M. Cotta, Natural convection inside two-dimensional cavities: the integral transform method, Commun. Numer. Meth. Eng. 15 (1999) 113–125.
[21] J.S. Perez Guerrero, J.N.N. Quaresma, R.M. Cotta, Simulation of laminar flow inside ducts of irregular geometry using integral transforms, Comput. Mech. 25 (4) (2000) 413–420.
[22] S. Wolfram, The Mathematica Book, 3rd ed., Wolfram Media, Cambridge University Press, Cambridge, 1996.
[23] S. Chandrasekhar, W.H. Reid, On the expansion of functions which satisfy four boundary conditions, In: Proc. Nat. Acad. Sci., 43, 1957, pp. 521–527.
[24] IMSL Library, Math/Lib., Houston, TX, 1989.